

Destructible Bars in Disk Galaxies under the Dynamical Influence of a Massive Central Black Hole

Shunsuke HOZUMI

Faculty of Education, Shiga University, 2-5-1 Hiratsu, Otsu, Shiga 520-0862
 hozumi@edu.shiga-u.ac.jp

(Received 2011 April 11; accepted 2011 August 9)

Abstract

The characteristics of the galactic bars that are prone to suffer a damaging impact from a massive central black hole are examined using flat stellar disks. We construct three disk model groups that consist of exponential disks with one type of velocity distribution and Kuzmin-Toomre disks with two different types of exact equilibrium distribution function. For each disk model group, three disks that have different typical Toomre’s Q values are evolved to form bars through dynamical instability. Once a bar is fully developed, a black hole (BH), whose mass is 1% of the disk mass, is adiabatically added at the center of the disk. Our results show that lower-amplitude bars, that is, weaker bars are dissolved more easily by that BH. We have found that this destructibility is rooted in the characteristic feature that the bar formed spontaneously becomes shorter in length and rounder in shape with decreasing bar amplitude. Since such weaker bars are found to originate from colder disks in each disk model group, it follows that for a given form of velocity structure, the coldness of an initial disk determines whether the bar produced in that disk is favorable to dissolution induced by a massive central BH. In addition, the existence of bar-dissolved galaxies of the kind studied here is also discussed.

Key words: black hole physics — galaxies: evolution — galaxies: kinematics and dynamics — galaxies: structure — methods: n -body simulations

1. Introduction

The existence of the supermassive black holes, whose masses range from $\sim 10^6 M_\odot$ to $\sim 10^9 M_\odot$, that reside in the centers of disk galaxies is gaining a firm basis observationally (Magorrian et al. 1998; Tremaine et al. 2002; Marconi & Hunt 2003; Marconi et al. 2003, 2004; Häring & Rix 2004; Atkinson et al. 2005; Pastorini et al. 2007; Beifiori et al. 2009; Siopis et al. 2009). Such a large-mass black hole (BH) could dissolve a bar in a barred galaxy that embraces it, as a dynamical consequence. This kind of bar dissolution was first studied by Hasan and Norman (1990), who examined the stellar orbits moving in combined fixed potentials of a rotating bar and a central BH in two-dimensional configurations. Next, Hasan, Pfenniger, and Norman (1993) extended that work to three-dimensional configurations. Both studies showed that central mass concentrations like massive central BHs can destroy a bar by converting bar-supporting orbits into chaotic ones.

Although such orbital studies mentioned above are useful for understanding the mechanism of bar destruction, they cannot provide answers to the questions of how much BH mass is needed, and how long it takes, precisely to destroy a bar. As a helpful tool for resolving these issues, self-consistent N -body simulations have played an important role in investigating the detailed evolution of a bar under the influence of a massive central BH. As pioneering work on N -body studies, Norman, Sellwood, and Hasan (1996) explored the evolution of a Kuzmin-Toomre (K-T)

disk (Kuzmin 1956; Toomre 1963) both in two- and three-dimensional configurations in which a bar was formed by the bar instability, and then a BH was added at the center of the disk as an external field. They showed that regardless of disk geometries, the minimum BH mass required for bar destruction is 4–5% of the disk mass. Subsequently, Shen and Sellwood (2004) have obtained a similar BH mass to destroy a bar with high-quality N -body simulations using a three-dimensional K-T disk embedded in a halo.

Unfortunately, K-T disks are inadequate in that real disk galaxies are well-described by exponential surface-density distributions (Freeman 1970). Then, Hozumi and Hernquist (2005, hereafter HH) adopted a two-dimensional exponential disk and examined the effect of a central BH on a bar generated in that disk. Although the motions of stars in their simulations are restricted to a single plane, they have demonstrated that a BH with a mass of only 0.5% of the disk mass is sufficient for bar dissolution. This BH mass is about an order of magnitude smaller than that obtained by Norman et al. (1996) and that by Shen and Sellwood (2004). Concerning this difference, HH argued that since exponential disks are more centrally concentrated than K-T disks, central BHs could have a more destructive impact on a bar in the former than in the latter, and that as a result, bars in exponential disks could be destructed more easily. However, Athanassoula, Lambert, and Dehnen (2005, hereafter ALD) have shown that complete bar destruction needs a BH with a mass of at least 5% of the disk mass even for more realistic

models that are composed of an exponential disk and its surrounding live halo. Their result suggests that the difference in the minimum BH mass does not necessarily originate from the difference in the mass profile of the disks. Consequently, the discrepancy in the minimum BH mass still remains unexplained, although the difference in disk geometry and situation between the two studies might be related to that difference in the BH mass: HH used a two-dimensional disk without a halo, while ALD adopted a three-dimensional disk with a live halo.

If the BH mass required for destroying a bar is at least about 5% of the disk mass, bar dissolution of the kind stated here would be practically impossible. This is because the corresponding BH mass amounts to approximately $10^{9.5} M_\odot$ for a typical disk galaxy, while the largest BH mass derived observationally from nearby spiral galaxies is about $10^9 M_\odot$ (Kormendy 1988; Kormendy et al. 1996; Marconi & Hunt 2003). On the other hand, if that mass is around 0.5% of the disk mass, we can expect the existence of bar-dissolved galaxies in the real Universe. In this case, as Larson (2010) has argued, dissolving a bar could weaken and ultimately cease the central activities of disk galaxies, since a barred structure is considered effective in fueling gas into the nucleus and this gas inflow could drive such activities. Therefore, also from this viewpoint, it is significant to determine the precise lower limit of the BH mass for bar destruction in order to reveal the secular evolution of the barred galaxies that harbor central BHs. However, it is conceivable that the BH mass needed to destroy a bar depends on the characteristics of the bar. Indeed, the bars formed by the bar instability will have a diversity of shapes and structures that arise from the difference in the kinematic structure of the disk like that represented by Toomre's (1964) Q profile, even though its mass profile is fixed. Nevertheless, in the previous N -body studies noted above, the kinematic structure of the disk for a given mass profile was never changed systematically, with other parameters of the system intact. Instead, some parameters included in the system such as a BH mass and a BH softening length were surveyed systematically for a disk with given mass and velocity profiles.

In this paper, we examine what type of bar is destroyed easily by a massive central BH, and thereby aim at understanding what causes that difference in the minimum BH mass required for bar dissolution which has been described above. In section 2, we show disk models with different kinematic structures for given mass profiles in order to produce a wide variety of bars. In addition, a BH model is also provided. Our numerical method is described in section 3. In section 4, we present the evolution of the disk models, in which bars form spontaneously and then they are deformed by adding a BH at the center of the disk. The properties of the bars are disclosed as well. In section 5, we discuss destructible bars under the dynamical influence of a massive central BH. Conclusions are given in section 6.

2. Models

We adopt infinitesimally thin stellar disks in order to avoid another damaging influence on a bar arising from the fire-hose instability inherent in three-dimensional disks (Raha et al. 1991; Debattista et al. 2004; Martinez-Valpuesta & Shlosman 2004). In addition, we do not include bulge and halo components. Two different mass profiles for such flat disks are employed, that is, exponential and Kuzmin-Toomre disks that are globally unstable to the formation of a bar. On the other hand, as an external field, we model a BH that is placed at the center of the disk after the full growth of a bar.

2.1. Exponential Disks

The surface-density distributions of exponential disks, μ_{exp} , are given by

$$\mu_{\text{exp}}(R) = \frac{M_d}{2\pi h^2} \exp(-R/h), \quad (1)$$

where M_d is the mass of the disk, h is the scale length, and R is the distance from the center of the disk. The disks are truncated at $R = 10h$. As adopted by HH, the full phase space is realized with the method devised by Hernquist (1993), in which the velocity structure is approximated using moments of the collisionless Boltzmann equation. In so doing, following the observations of disk galaxies (van der Kruit & Searle 1981; Lewis & Freeman 1989), we determine the square of the radial velocity dispersion, σ_R^2 , so as to be proportional to the surface density such that

$$\sigma_R^2(R) = \sigma_0^2 \exp(-R/h), \quad (2)$$

where σ_0 is the radial velocity dispersion at the center. Although the initial models thus constructed are not based on exact equilibrium distribution functions, we did not see any violent changes in the early stages of evolution. This behavior indicates that these models are sufficiently close to exact dynamical equilibrium.

We set up three models that have different Toomre's (1964) Q profiles shown in figure 1a. These models are named models E1, E2, and E3, whose reference Q values at the supposed solar radius, $2.43h$ (8.5 kpc, see below), are 1.2, 0.91, and 0.64, respectively. As explained by Hernquist (1993), there is difficulty in completely fulfilling the σ_R^2 distribution given by equation (2) near the center, so that some reduction in σ_R^2 is needed within a certain radius. As a result, the σ_R^2 profiles of the models created here are not shifted vertically to one another at small radii. This behavior applies also to the Q profiles of the models, taking into consideration the definition of the Q parameter. Accordingly, model E1 has a rather different Q profile at small radii than models E2 and E3. Thus, in this disk model group, except at small radii, the functional form of the velocity structure is the same, and the radial velocity dispersion at each radius is different from model to model by a constant factor.

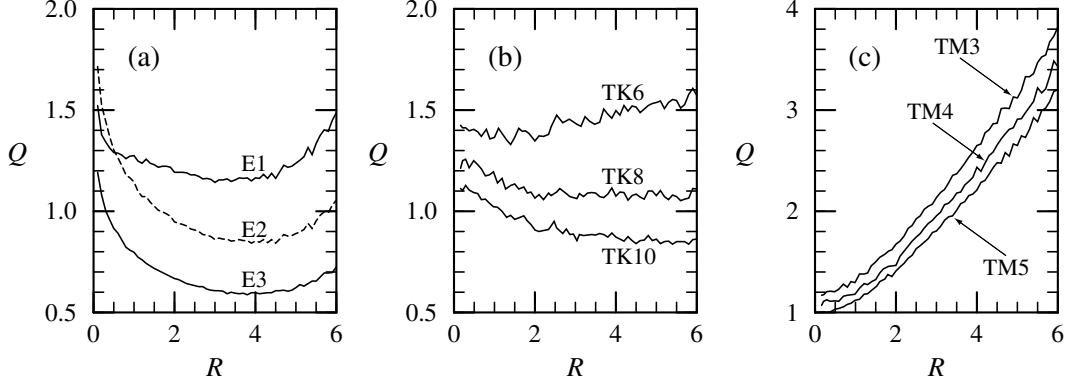


Fig. 1. Toomre's Q parameters as a function of radius for (a) models E1, E2, and E3 of the exponential disks, (b) models TK6, TK8, and TK10 of the Kuzmin-Toomre disks with Kalnajs's distribution functions, and (c) models TM3, TM4, and TM5 of the Kuzmin-Toomre disks with Miyamoto's distribution functions. Note that Q values at small radii for model E1 are smaller than those for model E2. Here, the radius is normalized by the exponential scale length h .

2.2. Kuzmin-Toomre Disks

The surface-density distributions of Kuzmin-Toomre (K-T) disks, μ_{KT} , are provided by

$$\mu_{KT}(R) = \frac{M_d}{2\pi h^2} \left(1 + \frac{R^2}{h^2}\right)^{-3/2}. \quad (3)$$

The disks are again truncated at $R = 10h$.

In contrast to the exponential disks, the K-T disks are known to possess exact equilibrium distribution functions (DFs), F_0 , in analytical forms. In general, for a flat axisymmetric galaxy, the equilibrium DF of directly rotating stars, F^+ , is composed of the energy, ε , and angular momentum, j , of a star per unit mass. This prograde part of the equilibrium DF, $F^+(\varepsilon, j)$, has been given by Kalnajs (1976) and by Miyamoto (1971). Here, we use both of the DFs.

On the other hand, there is no definite way of prescribing the distribution of retrograde stars. Then, we introduce them in the same manner as that adopted by Nishida et al. (1984). Consequently, the equilibrium DF is written as

$$F_0(\varepsilon, j) = \begin{cases} (1/2)F_0^+(\varepsilon) + F_1^+(\varepsilon, j) & j \geq 0, \\ (1/2)F_0^+(\varepsilon) & j < 0, \end{cases} \quad (4)$$

where the functions $F_0^+(\varepsilon)$ and $F_1^+(\varepsilon, j)$ are derived from the expansion of $F^+(\varepsilon, j)$ as

$$F^+(\varepsilon, j) = F_0^+(\varepsilon) + F_1^+(\varepsilon, j). \quad (5)$$

The two types of DF described above involve a model parameter that assigns the kinematic structure to the disk. When denoting this parameter as m_K for Kalnajs's DFs and as m_M for Miyamoto's DFs, we take $m_K = 6, 8$, and 10 , which are termed models TK6, TK8, and TK10, respectively, and $m_M = 3, 4$, and 5 , which are named models TM3, TM4, and TM5, respectively. We present the Q profiles for models TK6, TK8, and TK10 in figure 1b, and those for models TM3, TM4, and TM5 in figure 1c. The models generated from Kalnajs's DFs have slightly declining Q distributions with radius except for model TK6 that shows a slight increase in Q from $R \sim 1.3h$ with radius,

while those from Miyamoto's DFs yield steeply rising Q distributions with radius. At any rate, as the model parameters, m_K and m_M , increase, the Q values at all radii decrease for both DFs.

In these disk models, the functional form of the velocity structure is completely different between these two types of DF. For Miyamoto's DFs, the square of the radial velocity dispersion is represented by

$$\sigma_R^2(R) = -\frac{\Phi_{KT}(R)}{2m_M + 4}, \quad (6)$$

where Φ_{KT} is the potential of the K-T disk. Thus, in this disk model group, the radial velocity dispersion at each radius is different from model to model by a constant factor that depends on the model parameter m_M , so that the Q profiles are shifted vertically to one another, as is obvious in figure 1c. On the other hand, Kalnajs's DFs lead to rather complicated functional forms of the radial velocity dispersion. Even so, the resulting Q profiles show sequential changes designated by the model parameter m_K , as seen from figure 1b.

2.3. Black Hole

A black hole (BH) model is the same as that employed by HH. That is, a BH is represented by a softened point-mass using a spline-kernel (Hernquist & Katz 1989), and its scale length is set to be $0.01h$.

The BH is added at time t_{BH} after a bar is fully developed. To avoid a sudden change in the dynamical state of the disk caused by an addition of the BH, we increase the BH mass, $M_\bullet(t)$, from 0 to M_{BH} gradually with time t as follows:

$$M_\bullet(t) = \begin{cases} M_{BH}\tau^2(3-2\tau) & 0 \leq \tau \leq 1, \\ M_{BH} & \tau > 1, \end{cases} \quad (7)$$

where $\tau = (t - t_{BH})/t_{grow}$, and t_{grow} is the time for the BH to attain to its preassigned mass M_{BH} . Thus, the BH is made to grow adiabatically by taking t_{grow} to be sufficiently long. In our dimensionless system of units described in the next section, we choose t_{grow} to be 100, and set t_{BH} to be 200.

According to recent observations, the Sa galaxy NGC 4594 (Kormendy 1988; Marconi & Hunt 2003) and the S0 galaxy NGC 3115 (Kormendy et al. 1996) are thought to harbor a central BH with a mass of approximately $10^9 M_\odot$, which is the largest BH mass inferred in nearby spirals. Since this BH mass is close to 1% of the disk mass for a typical disk galaxy, we set $M_{\text{BH}} = 0.01 M_d$. With this choice, we can evaluate the largest impact of a central BH on a bar from a realistic point of view.

3. Method

We use a self-consistent field (SCF) method (Hernquist & Ostriker 1992) to follow the evolution of the disks constructed in the previous section and that of the systems including the BH. In this approach, Poisson's equation is solved by expanding the surface density, μ , and potential, Φ , of the disk in a bi-orthogonal basis set such that

$$\mu(\mathbf{R}) = \sum_{nm} A_{nm}(t) \mu_{nm}(\mathbf{R}) \quad (8)$$

and

$$\Phi(\mathbf{R}) = \sum_{nm} A_{nm}(t) \Phi_{nm}(\mathbf{R}), \quad (9)$$

where μ_{nm} and Φ_{nm} are, respectively, the surface-density and potential basis functions, A_{nm} are the expansion coefficients, and \mathbf{R} is the position vector. In the SCF code, we adopt Aoki and Iye's (1978) basis set that is suitable for flat stellar disks. The outline of SCF simulations is explained by Hernquist and Ostriker (1992) and by Hozumi (1997). In addition, the computational details concerning the simulations presented here are described by HH.

The disks are realized with $N = 1,000,000$ particles of equal mass. The equations of motion are integrated in Cartesian coordinates with a time-centered leapfrog algorithm (e.g., Press et al. 1986). We present results in the system of units such that $G = M_d = h = 1$, where G is the gravitational constant. These units can be scaled to physical values appropriate for the Milky Way using $h = 3.5$ kpc and $M_d = 5.6 \times 10^{10} M_\odot$, with the result that unit time and velocity are 1.31×10^7 yr and 262 km s^{-1} , respectively.

We set the maximum numbers of radial and azimuthal expansion terms in the SCF code, n_{max} and m_{max} , respectively, to be $n_{\text{max}} = 24$ and $m_{\text{max}} = 12$. In imposing these numbers of the expansion terms on each model, we save only even m -values to avoid a sizable disagreement between the center of the bar and the position of the BH caused by asymmetric features that would originate from odd m -values. Again, the computational details are taken over from those stated by HH.

Although our present simulations include a wide range of timescales after introducing the BH, we use a fixed time step that is made as small as possible. In order to reduce computation times, we have parallelized the SCF code in accordance with the prescription provided by Hernquist, Sigurdsson, and Bryan (1995) (see also Holley-Bockelmann et al. 2001). The time steps adopted are

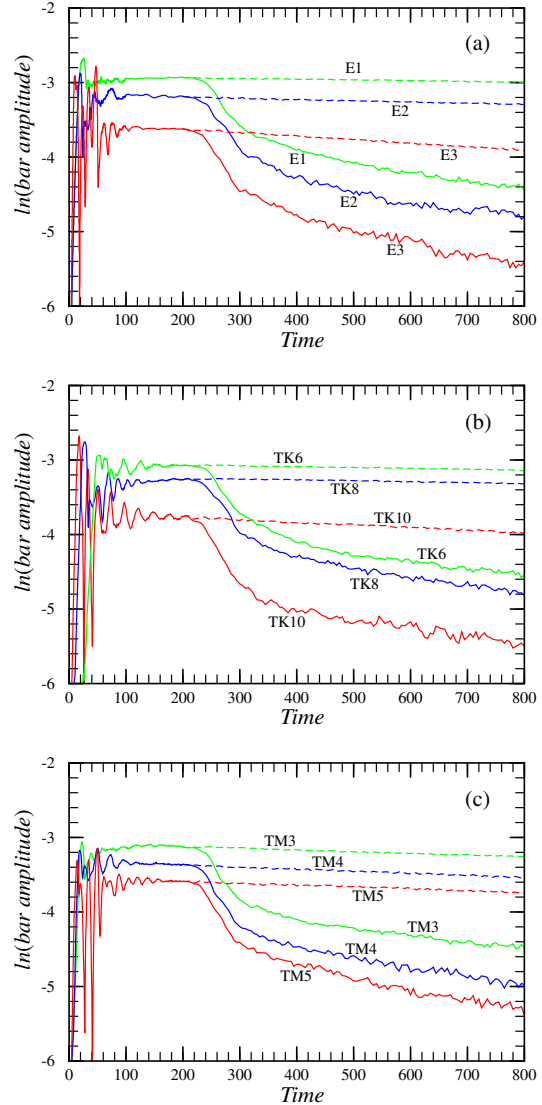


Fig. 2. Time evolution of the bar amplitude before and after the addition of the black hole (solid lines) for (a) models E1, E2, and E3 of the exponential disks, (b) models TK6, TK8, and TK10 of the Kuzmin-Toomre disks with Kalnajs's distribution functions, and (c) models TM3, TM4, and TM5 of the Kuzmin-Toomre disks with Miyamoto's distribution functions. The black hole is added at $t = 200$, and grows up fully at $t = 300$. The bar evolution without the black hole after $t = 200$ is also shown with dashed lines for each model.

$\Delta t = 0.05$ and $\Delta t = 0.002$ before and after the addition of the BH, respectively. With these choices of time step, the relative energy error of the system after the full growth of the BH was, in all cases, smaller than 7.2×10^{-6} .

4. Results

4.1. Evolution of Bars

As the disks are evolved forward in time, linearly growing two-armed spiral modes excited in the disks are deformed into bars in nonlinear regimes through the bar instability. We evaluate the bar amplitude by the absolute value of the expansion coefficient, $|A_{22}(t)|$, which

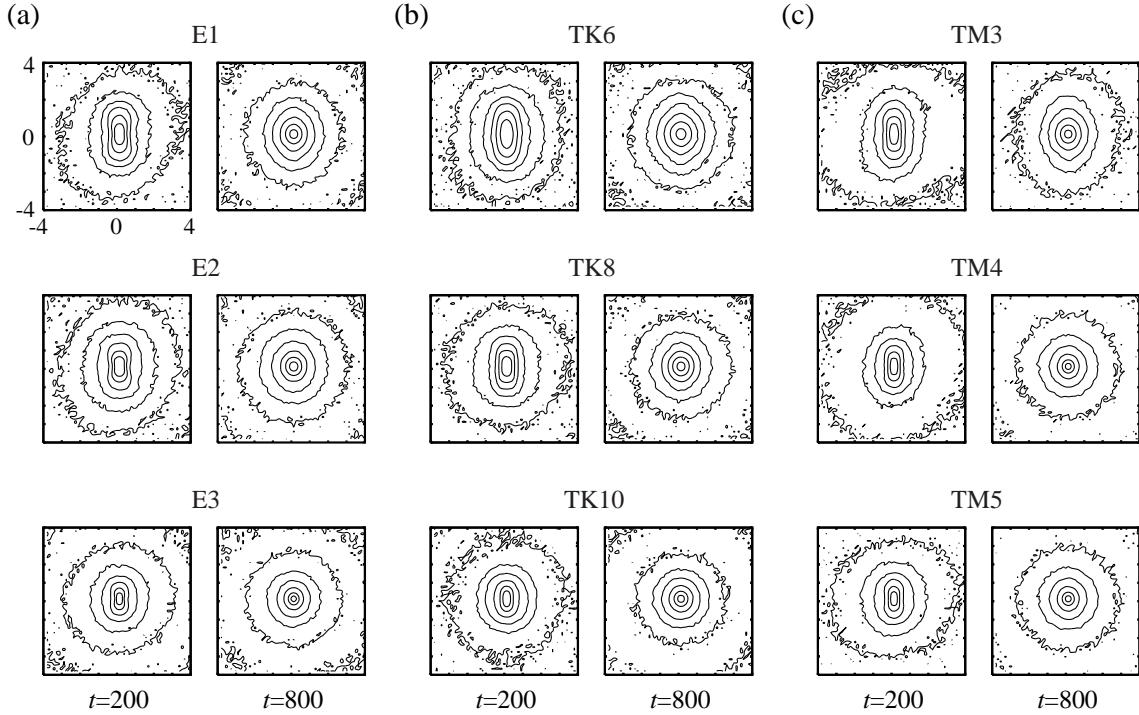


Fig. 3. Density contours in barred structures at the time just before the addition of the black hole ($t = 200$) and at the end of the simulations ($t = 800$) for (a) models E1, E2, and E3 of the exponential disks, (b) models TK6, TK8, and TK10 of the Kuzmin-Toomre disks with Kalnajs's distribution functions, and (c) models TM3, TM4, and TM5 of the Kuzmin-Toomre disks with Miyamoto's distribution functions. The bar major axis is aligned to the y axis. The contour levels are drawn at the 90, 80, 70, \dots , and 30% of the peak amplitude on logarithmic scales. Black hole growth starts at $t = 200$ and ends at $t = 300$. All patterns rotate counterclockwise.

corresponds to the amplitude of the fastest growing two-armed mode (see HH). Figure 2 shows the time evolution of the bar amplitude for each model of the three disk model groups. From this figure, we find that all bars are fully developed at least by $t = 200$, and that their amplitudes are practically held constant over time to the end of the simulations unless the BH is added, although in an exact sense, some bars grow in amplitude very slightly with time and others show small decrements in amplitude with time, in response to a way of redistributing the angular momentum of a bar. We have thus chosen the time of adding the BH to be $t_{\text{BH}} = 200$, as mentioned in section 2.3. We notice from figure 2, along with figure 1, that in each disk model group, the bar amplitude becomes lower as the disk is colder in the sense of typical Q values. Concerning the exponential disks, the bar amplitude of model E1 is larger than that of model E2, while Q values at small radii for model E1 are slightly smaller than those for model E2 as expressed in figure 1. This fact implies that the bar amplitude would not be sensitive to the inner velocity structures but to the relatively outer ones.

Once the BH is added at $t = t_{\text{BH}}$, the bar amplitudes start to decrease with time, as demonstrated in figure 2. After the full growth of the BH, the bar amplitudes continue to decay almost exponentially with time till the end of the simulations. Consequently, the bars become very round in the final stages as found from a comparison between the density contours at $t = t_{\text{BH}}$ and those at the end of the simulations, which are illustrated in figure 3.

To quantify to what degree the bars are made round, we evaluate the axis ratios of the bars along radius at these two times by calculating the principal moment of inertia tensor for particles included in a specified radius, the value of which is regarded as the axis ratio at that radius. Resulting axis-ratio profiles are presented in figure 4. We can see from this figure, together with figure 3, that in each disk model group, the bar is more easily deformed into a rounder shape as the smallest axis ratio along radius is larger, that is, the bar is rounder when the BH is added, or as the bar half-length, estimated here to be a distance from the center to the radius of the smallest axis ratio, is shorter.

Since the final axis ratios of the bars exceed about 0.9 at all radii except for the bar of model TM3 (the final axis ratio is 0.86), irrespective of the mass and velocity profiles, it follows that a BH with a mass of 1% of the disk mass can destroy almost completely, or in some cases appreciably, the bars formed by the bar instability. Furthermore, when we take into account the Q profiles shown in figure 1, the runs of the final axis ratios in figure 4 indicate that in each disk model group, the bars originating from the colder disks are destroyed more easily by the BH.

4.2. Characteristics of Bars

We describe the characteristics of the bars before the BH acts on them to unravel what type of bar is more destructible under the dynamical influence of a massive central BH.

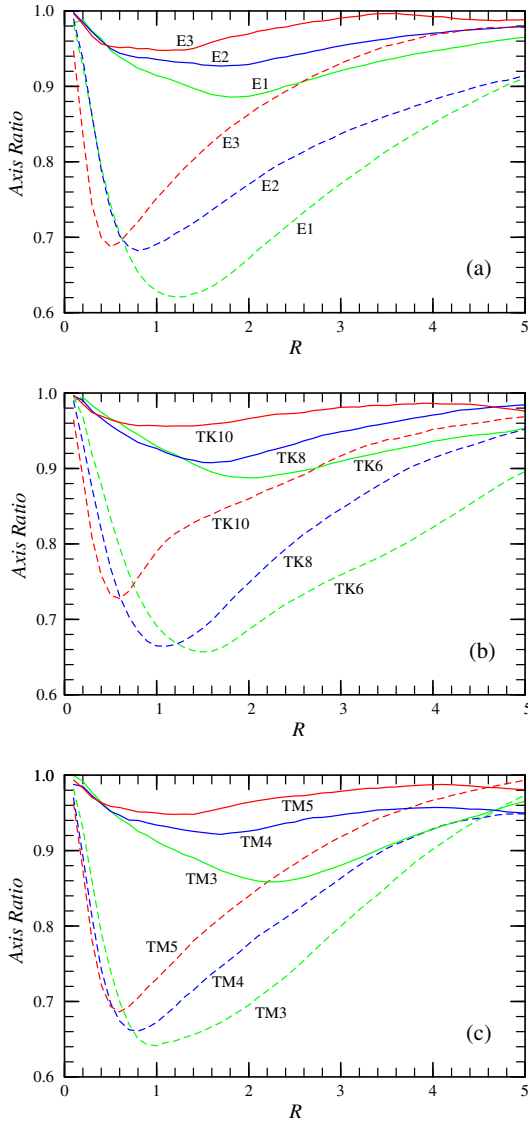


Fig. 4. Axis ratio of bars as a function of radius for (a) the exponential disks, (b) the Kuzmin-Toomre disks with Kalnajs's distribution functions, and (c) the Kuzmin-Toomre disks with Miyamoto's distribution functions. Dashed lines show the axis ratios of the bars just before the black hole is added ($t = 200$), while solid lines represent those at the end of the simulations ($t = 800$).

Figure 5 presents the surface-density profiles of the bars along the major and minor axes at $t = t_{\text{BH}}$ just before the BH is added. Except for models E1 and TK6, there is no noticeable change in the density slope on logarithmic scales from the center towards the bar ends along the major axis. On the other hand, models E1 and TK6 show a bend in the surface-density distribution along the major axis at around an intermediate position between the center and the bar end, although the bend for model TK6 is rather gentle as compared to that for model E1. The surface-density profiles along the minor axis for these two models are close to those of the rest of the models.

To examine the structures of the bars in detail, we analyze the surface-density profiles by calculating their

Fourier components along radius, $I_m(R)$, where $m = 2, 4, 6$, and 8. These Fourier components are normalized by the $m = 0$ component, I_0 , of the disk being analyzed. The resulting relative Fourier amplitudes of each model at $t = t_{\text{BH}}$ are displayed in figure 6. Here, we calculate the Fourier components in the same manner as that done by Ohta, Hamabe, and Wakamatsu (1990) and by Athanassoula and Misiriotis (2002). This figure indicates that for the hottest models in each disk model group from a viewpoint of typical Q values, that is, for models E1, TK6, and TM3, the amplitudes for the $m = 4$ and $m = 6$ components are large in magnitude as well as for the $m = 2$ component, while for the rest of the models they are small, and, in particular, the amplitudes for the $m = 6$ component are negligibly small. In addition to this property of the hottest models, taking into account the Q profiles presented in figure 1, together with figure 5, we can see that a bend in the surface-density distribution of the bar along the major axis is produced for the models that have relatively high Q values near the center as for models E1 and TK6.

To further characterize the bars, we measure the size of the bar region at $t = t_{\text{BH}}$, following Ohta et al. (1990), who defined the bar region to be the region where the value of $(I_0 + I_2 + I_4 + I_6)/(I_0 - I_2 + I_4 - I_6)$ exceeds 2.0. In figure 7, the measured size of the bar region (bar half-size) is plotted against the bar amplitude that is normalized by the amplitude of the ring mode ($m = 0$), $|A_{22}|/|A_{00}|$, at $t = t_{\text{BH}}$ in order to be compared among the disk models with the different mass and velocity profiles. This figure reveals that the bar size is approximately proportional to the normalized bar amplitude.

As another ingredient for featuring the bars, the smallest axis ratio along radius at $t = t_{\text{BH}}$, as a measure of the degree of elongation, is plotted against the normalized bar amplitude in figure 8. We can find from this figure that on the whole, the roundness of the bar decreases monotonically with increasing normalized bar amplitude.

5. Discussion

We have obtained a wide variety of bars from the exponential and K-T disks to which various velocity distributions are assigned. The amplitude of these bars continues to decay exponentially with time till the end of the simulations after the full growth of the BH that is added at the center of the disk. When we pay attention to the three models of each disk model group, the final axis-ratio profiles in figure 4 show that the BH can make the bar rounder as the bar amplitude becomes lower. To be sure, it may be no wonder that lower-amplitude bars are destructed more easily by a given mass BH. The important thing is that this fragility of low-amplitude bars originates from the bar properties exposed in figures 7 and 8 that the normalized bar amplitude is related to the size and shape of a bar. Therefore, the precise explanation is that since lower-amplitude bars are shorter in length and rounder in shape, a given mass BH can provide a more destructive impact on shorter bars that lie more deeply

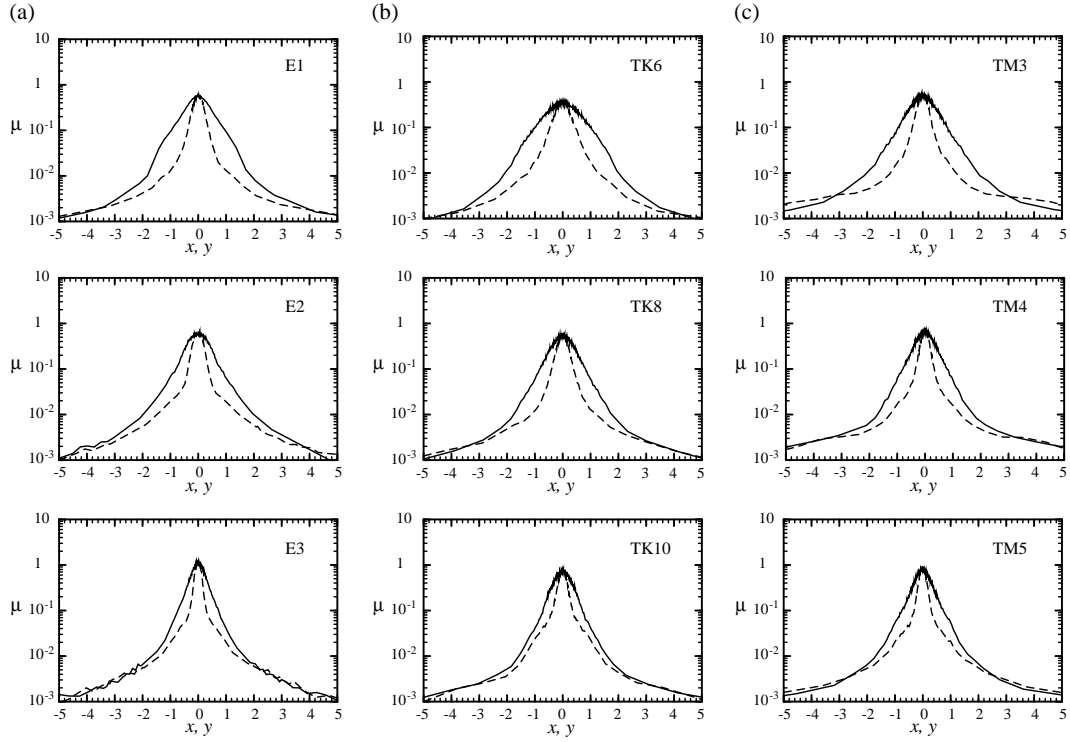


Fig. 5. Surface-density profiles along the major (solid lines) and minor (dashed lines) axes at the time just before the black hole is added ($t = 200$) for (a) models E1, E2, and E3 of the exponential disks, (b) models TK6, TK8, and TK10 of the Kuzmin-Toomre disks with Kalnajs's distribution functions, and (c) models TM3, TM4, and TM5 of the Kuzmin-Toomre disks with Miyamoto's distribution functions.

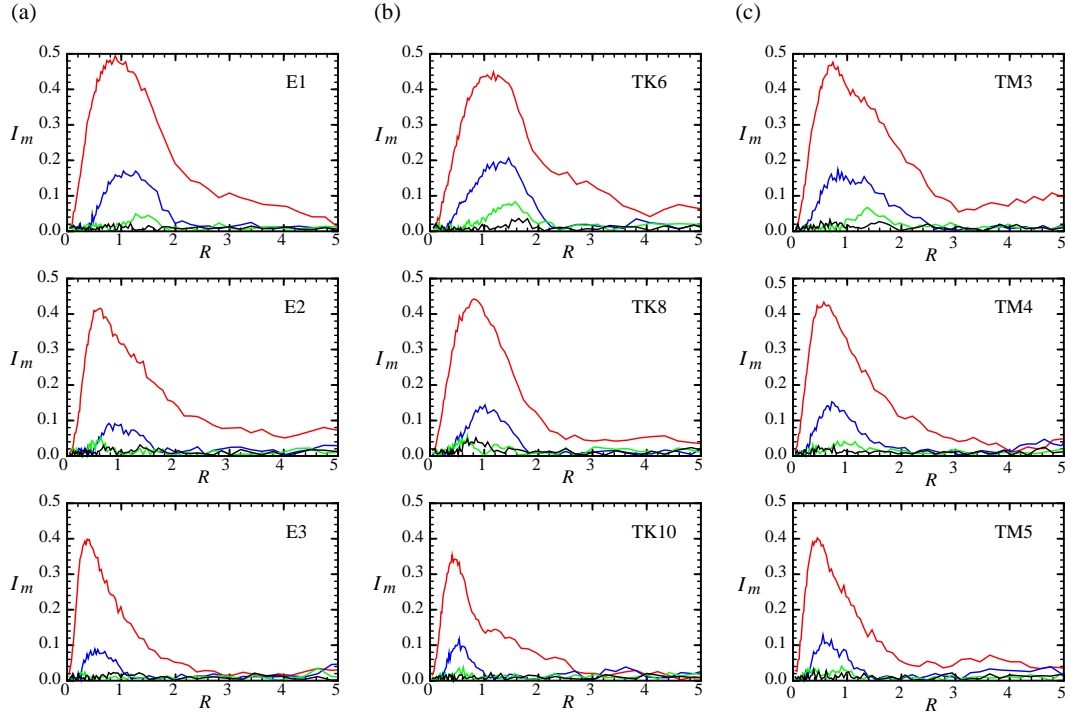


Fig. 6. Fourier amplitudes of the surface-density distribution, I_m , for the $m = 2$ (red lines), 4 (blue lines), 6 (green lines), and 8 (black lines) components normalized by the $m = 0$ component at the time just before the black hole is added ($t = 200$) as a function of radius for (a) models E1, E2, and E3 of the exponential disks, (b) models TK6, TK8, and TK10 of the Kuzmin-Toomre disks with Kalnajs's distribution functions, and (c) models TM3, TM4, and TM5 of Kuzmin-Toomre disks with Miyamoto's distribution functions.

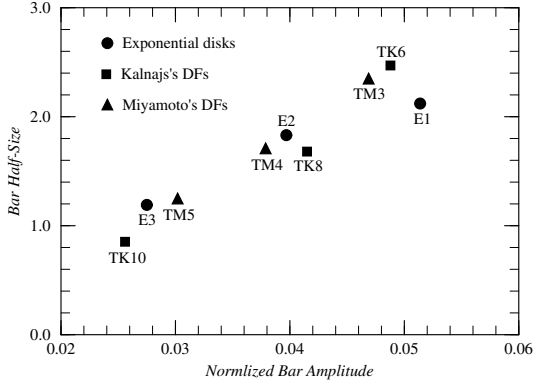


Fig. 7. Bar half-size as a function of bar amplitude normalized by the amplitude of the ring mode excited in each model disk. The bar half-size and the amplitudes of the bar and ring modes are calculated at the time just before the addition of the black ($t = 200$). The definition of the bar half-size is described in the text.

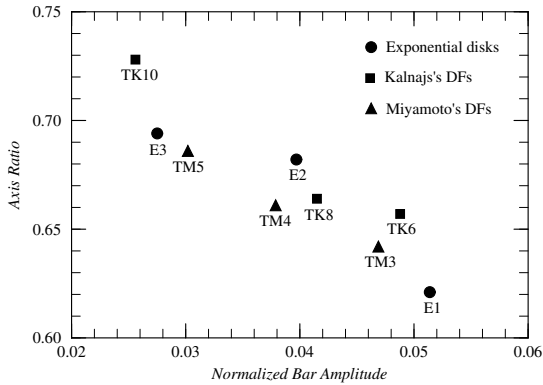


Fig. 8. Axis ratio of bars as a function of bar amplitude normalized by the amplitude of the ring mode excited in each model disk. The axis ratio means the smallest axis ratio along radius for each model. The axis ratio and the amplitudes of the bar and ring modes are calculated at the time just before the addition of the black hole ($t = 200$).

inside the BH's “sphere of influence”, and can increase the roundness more easily for rounder bars over a given period.

We should mention the bar properties extracted in the present study from an observational point of view. Elmegreen et al. (2007) have found from K_s -band images of barred galaxies that longer bars have higher bar amplitudes. On the other hand, analyzing near-infrared images of nearby barred galaxies, Menéndez-Delmestre et al. (2007) have indicated a weak tendency that the bar ellipticity is larger for longer bars. Here, the bar ellipticity is defined as $1 - b/a$, where b/a is the axis ratio of a bar. Also, very recently, Hoyle et al. (2011) have presented a similar correlation between the bar ellipticity and bar length from an analysis of bar length measurements in local disk galaxies. Then, if we are allowed to combine these two kinds of observed results, we are led to the conclusion that the bar ellipticity increases with increasing bar amplitude. In fact, the bar ellipticity is often

used as a measure of the bar strength: larger bar ellipticities mean higher bar amplitudes (Chapelon, Contini, & Davoust 1999; Laine et al. 2002; Laurikainen, Salo, & Rautiainen 2002). Therefore, the properties that we have uncovered for the simulated bars are consistent with those of real barred galaxies. Although the correlation of the bar length and ellipticity with the bar amplitude has thus far been explained from a viewpoint of secular evolution (Elmegreen et al. 2007; Menéndez-Delmestre et al. 2007; Hoyle et al. 2011), we will demonstrate in a future paper that these bar properties are closely related to the properties of the fastest growing, globally unstable two-armed modes excited in stellar disks, which finally lead to bars in nonlinear regimes.

We have also found that the lower-amplitude bars are generated from the colder disks in each disk model group, although the physical origin of this finding is unclear at the moment (we will mention it also in that future paper). Consequently, once the functional form of the velocity distribution is assigned, the degree of the coldness of a disk determines the fragility of a bar under the dynamical influence of a massive central BH at least for two-dimensional disks. If this property is applicable to bars formed in three-dimensional disks, the discrepancy that HH's minimum BH mass necessary for bar dissolution in the exponential disk is about an order of magnitude smaller than ALD's one might have arisen partly from the difference in the coldness, more precisely, the Q profile of the disk. However, it is uncertain whether the relation between the coldness of a disk and the amplitude of a bar holds for bars produced in three-dimensional disks, because the fire-hose instability intrinsic in such disks (Raha et al. 1991; Debattista et al. 2004; Martinez-Valpuesta & Shlosman 2004) and bar-halo interactions (Athanasoula 2002; Athanasoula & Misiriotis 2002), both of which are not included in the present study, might distort those properties of the bars which have been obtained in flat disks. Thus, we need to investigate the validity of this relation using realistic disk galaxy models in three-dimensional configurations.

Note that the relation between the coldness of a disk and the fragility of a bar mentioned above is obtained by ignoring the effects of gas components on the bar instability, because our simulations are based on pure stellar dynamics. In general, if gas components are added to a stellar disk, the system will become colder on account of their low velocity dispersions. Then, we could expect a lower-amplitude bar in such a system that would suffer a more violent bar instability. In a case where a large gas mass fraction is included in a disk, Shlosman and Noguchi (1993) demonstrated that the bar instability in the disk is damped heavily. Even in this situation, it can be interpreted apparently that an extremely weak bar or bar-like structure is formed in an exceedingly cold disk owing to a large amount of gas. Thus, in principle, our finding that colder disks lead to lower-amplitude bars might hold even for the disks that contain gas components, regardless of their amount.

Figures 5 and 6 have indicated that robust bars against

the dynamical influence of a massive central BH have relatively larger Fourier amplitudes for the $m = 4$ and $m = 6$ components (models E1, TK6, and TM3), and that for the models whose Q values are somewhat large near the center (models E1 and TK6), the bars represented by these Fourier components exhibit a bend in the surface-density profile along the major axis. These two features appear similar to those of the MH-type models, employed by Athanassoula (2002) and by Athanassoula and Misiriotis (2002), whose halos are characterized by small core radii. On the other hand, the surface-density profiles of the models other than models E1 and TK6 have no noticeable change in density slope along the bar major axis. This feature corresponds to that obtained from the MD-type models, also used by Athanassoula (2002) and by Athanassoula and Misiriotis (2002), whose halos are depicted by large core radii. ALD have reported that for a given mass central BH, bars formed in the MH-type models are less destructible than those in the MD-type models. Interestingly, ALD mentioned that the disks in the MH-type models have $Q = 1.4$, while those in the MD-type models have $Q = 1$. Thus, this relation between the degree of bar destruction and the typical Q value is in concord with our claim that bars formed in colder disks are more destructible. It is true that we cannot compare directly between their results and ours, since the disks in their MH- and MD-type models are three-dimensional and their halos are self-gravitating, while our models are two-dimensional and have no halos. Nevertheless, our models seem to reflect the characteristics possessed by the bars in their MH- and MD-type models. This finding may imply that the velocity structure of the disk affects more substantially the characteristics of the bars formed by the bar instability than the difference in the central concentration of self-gravitating halos. Therefore, we should examine the bar properties for both MH- and MD-type models that have a wide variety of velocity structures in the disks, and evaluate the minimum BH mass needed to dissolve the bars formed spontaneously. This line of investigation will enable us to confirm whether the discrepancy in the minimum BH mass between HH's study and the others is due to the difference in the velocity structure of the disk.

HH argued that the destructive effect of a central BH on a bar could be considered stronger for more centrally concentrated disks. Although Norman et al. (1996) used a K-T disk and ALD adopted an exponential disk, both studies resulted in a similar BH mass that is about 5% of the disk mass as the minimum value required for bar dissolution, in spite of the fact that exponential disks are more centrally concentrated than K-T disks. This result might suggest that the velocity structure is more significant to bar dissolution than the degree of mass concentration of the disk, because our simulations have shown that the vulnerability of a bar to a given mass central BH depends on the velocity structure of the disk. Furthermore, we have found from figures 7 and 8 that the size and roundness of a bar are determined by the normalized bar amplitude, irrespective of the mass profile of the disk, and that the strength of this amplitude is connected to the destructibil-

ity of a bar. However, we cannot answer exactly whether these bar properties depend on the degree of mass concentration of the disk, since it is prohibitively difficult to construct such models that have the same velocity structure for different mass profiles. Therefore, we cannot conclude definitely that the bars generated in more centrally concentrated disks are destroyed more easily by a given mass central BH.

We have found that the bar amplitude continues to decrease almost exponentially with time for 500 time units after the full growth of the BH. This simulated period corresponds to about 7 Gyr, if the time unit is represented by the physical value appropriate for the Milky Way. We have also found that the bars formed in the exponential disks have been practically destroyed within that period by the BH whose mass is 1% of the disk mass. This BH mass is reduced to be approximately $10^9 M_\odot$ for a typical disk galaxy, and so, it is comparable to the largest mass for central BHs in nearby spirals (Kormendy 1988; Kormendy et al. 1996; Marconi & Hunt 2003). Therefore, our simulations suggest that bar dissolution induced by a massive central BH could occur in the real Universe, if galaxy disks are relatively cold at birth. However, the frequency of such bar dissolution would be rare, since the minimum BH mass examined by HH (about $10^{8.5} M_\odot$) as well as the BH mass in this work are close to the upper bound of the observationally derived BH masses. Consequently, the bar fraction would be declined to a negligible degree, if any, as the Universe evolves, by the bar dissolution mechanism studied here. In fact, Elmegreen, Elmegreen, and Hirst (2004) and Jogee et al. (2004) found that the observed bar fraction is nearly constant, and recently, Sheth et al. (2008) have shown that it even increases with time over the last 7 Gyr (see also Abraham et al. 1999; van den Bergh et al. 2002).

6. Conclusions

We have examined the properties of the bars formed by the bar instability in the exponential disks with approximate equilibrium velocity distributions and the Kuzmin-Toomre disks with two different types of exact equilibrium DF in two-dimensional configurations, and the damaging impact of a massive central BH on these bars. Then, we have found that lower-amplitude bars, that is, weaker bars are destroyed more easily by a given mass central BH, because the bar formed by the bar instability is shorter in length and rounder in shape as the bar amplitude decreases, thereby being more susceptible to the dynamical influence of that BH.

In addition, we have also found that lower-amplitude bars are generated from colder disks for a given functional form of the velocity distribution. This finding suggests that destructible bars under the dynamical influence of a given mass central BH are determined by the kinematic properties of disks, like those specified by typical Q values, at the formation epoch, once the functional form of the velocity distribution is assigned. Thus, it is likely that the discrepancy in the lowest BH mass required for bar

dissolution found in the previous simulations might have resulted from the difference in the velocity structure of the disk.

When scaling the dimensionless units to appropriate physical values, we have shown that the bar amplitude continues to decrease almost exponentially with time for about 7 Gyr after the full growth of a BH, and that the bars formed in the relatively cold exponential disks have resulted in practical dissolution for a BH with a mass of approximately $10^9 M_\odot$, a likely largest BH mass derived observationally from nearby spirals. We thus infer that bar dissolution induced by a massive central BH could occur in the real Universe, if galaxy disks are formed in a rather cold state.

The author is indebted to Dr. K. Nitadori for optimizing the two-dimensional SCF code for parallelization. He would also like to thank the anonymous referee for the valuable comments that have called the author's attention to the connection of the present work to observations, which have helped improve the manuscript. Numerical computations were carried out on the PC cluster and Cray XT4 at the Center for Computational Astrophysics (CfCA), the National Astronomical Observatory of Japan.

References

- Abraham, R. G., Merrifield, M. R., Ellis, R. S., Tanvir, N. R., & Brinchmann, J. 1999, *MNRAS*, 308, 569
- Aoki, S., & Iye, M. 1978, *PASJ*, 30, 519
- Athanassoula, E. 2002, *ApJ*, 569, L83
- Athanassoula, E., Lambert, J. C., & Dehnen, W. 2005, *MNRAS*, 363, 496 (ALD)
- Athanassoula, E., & Misiriotis, A. 2002, *MNRAS*, 330, 35
- Atkinson, J. W., et al. 2005, *MNRAS*, 359, 504
- Beifiori, A., Sarzi, M., Corsini, E. M., Dalla Bontà E., Pizzella, A., Coccatto, L., & Bertola, F. 2009, *ApJ*, 692, 856
- Chapelon, S., Contini, T., & Davoust, E. 1999, *A&A*, 345, 81
- Debattista, V. P., Carollo, C. M., Mayer, L., & Moore, B. 2004, *ApJ*, 604, L93
- Elmegreen, B. G., Elmegreen, D. M., & Hirst, A. C. 2004, *ApJ*, 612, 191
- Elmegreen, B. G., Elmegreen, D. M., Knapen, J. H., Buta, R. J., Block, D. L., & Puerari, I. 2007, *ApJ*, 670, L97
- Freeman, K. C. 1970, *ApJ*, 160, 811
- Häring, N., & Rix, H.-W. 2004, *ApJ*, 604, L89
- Hasan, H., & Norman, C. 1990, *ApJ*, 361, 69
- Hasan, H., Pfenniger, D., & Norman, C. 1993, *ApJ*, 409, 91
- Hernquist, L. 1993, *ApJS*, 86, 389
- Hernquist, L., & Katz, N. 1989, *ApJS*, 70, 419
- Hernquist, L., & Ostriker, J. P. 1992, *ApJ*, 386, 375
- Hernquist, L., Sigurdsson, S., & Bryan, G. L. 1995, *ApJ*, 446, 717
- Holley-Bockelmann, K., Mihos, J. C., Sigurdsson, S., & Hernquist, L. 2001, *ApJ*, 549, 862
- Hoyle, B., et al. 2011, *MNRAS*, accepted
- Hozumi, S. 1997, *ApJ*, 487, 617
- Hozumi, S., & Hernquist, L. 2005, *PASJ*, 57, 719 (HH)
- Jogee, S., et al. 2004, *ApJ*, 615, L105
- Kalnajs, A. J. 1976, *ApJ*, 205, 751
- Kormendy, J. 1988, *ApJ*, 335, 40
- Kormendy, J., et al. 1996, *ApJ*, 459, L57
- Kuzmin, G. 1956, *AZh.*, 33, 27
- Laine, S., Shlosman, I., Knapen, J. H., & Peletier, R. F. 2002, *ApJ*, 567, 97
- Larson, R. B. 2010, *Rep.Prog.Phys.*, 73, 014901
- Laurikainen, E., Salo, H., & Rautiainen, P. 2002, *MNRAS*, 331, 880
- Lewis, J. R., & Freeman, K. C. 1989, *AJ*, 97, 139
- Magorrian, J., et al. 1998, *AJ*, 115, 2285
- Marconi, A., & Hunt, L. K. 2003, *ApJ*, 589, L21
- Marconi, A., et al. 2003, *ApJ*, 586, 868
- Marconi, A., Risaliti, G., Gilli, R., Hunt, L. K., Maiolino, R., & Salvati, M. 2004, *MNRAS*, 351, 169
- Martinez-Valpuesta, I., & Shlosman, I. 2004, *ApJ*, 613, L29
- Menéndez-Delmestre, K., Sheth, K., Schinnerer, E., Jarrett, T. H., & Scoville, N. Z. 2007, *ApJ*, 657, 790
- Miyamoto, M. 1971, *PASJ*, 23, 21
- Nishida, M. T., Watanabe, Y., Fujiwara, T., & Kato, S. 1984, *PASJ*, 36, 27
- Norman, C. A., Sellwood, J. A., & Hasan, H. 1996, *ApJ*, 462, 114
- Ohta, K., Hamabe, M., & Wakamatsu, K. 1990, *ApJ*, 357, 71
- Pastorini, G., et al. 2007, *A&A*, 469, 405
- Press, W. H., Flannery, B. P., Teukolsky, S. A., & Vetterling, W. T. 1986, *Numerical Recipes: The Art of Scientific Computing* (Cambridge: Cambridge University Press), 631
- Raha, N., Sellwood, J. A., James, R. A., & Kahn, F. D. 1991, *Nature*, 352, 411
- Shen, J., & Sellwood, J. A. 2004, *ApJ*, 604, 614
- Sheth, K., et al. 2008, *ApJ*, 675, 1141
- Shlosman, I., & Noguchi, M. 1993, *ApJ*, 414, 474
- Siopis, C., et al. 2009, *ApJ*, 693, 946
- Toomre, A. 1963, *ApJ*, 138, 385
- Toomre, A. 1964, *ApJ*, 139, 1217
- Tremaine, S., et al. 2002, *ApJ*, 574, 740
- van den Bergh, S., Abraham, R. G., Whyte, L. F., Merrifield, M. R., Eskridge, P. B., Frogel, J. A., & Pogge, R. 2002, *AJ*, 123, 2913
- van der Kruit, P. C., & Searle, L. 1981, *A&A*, 95, 105